

Hidden Markov graphical models with state-dependent generalized hyperbolic distributions

Beatrice Foroni¹, Luca Merlo², and Lea Petrella³

¹Department of Management and Economics, University of Pisa

²Department of Human Sciences, Link Campus University of Rome

³MEMOTEF Department, Sapienza University of Rome

December 6, 2024

Abstract

In this paper we develop a novel hidden Markov graphical model to investigate time-varying interconnectedness between different financial markets. To identify conditional correlation structures under varying market conditions and accommodate stylized facts embedded in financial time series, we rely upon the generalized hyperbolic family of distributions with time-dependent parameters evolving according to a latent Markov chain. We exploit its location-scale mixture representation to build a penalized EM algorithm for estimating the state-specific sparse precision matrices by means of an L_1 penalty. The proposed approach leads to regime-specific conditional correlation graphs that allow us to identify different degrees of network connectivity of returns over time. The methodology's effectiveness is validated through simulation exercises under different scenarios. In the empirical analysis we apply our model to daily returns of a large set of market indexes, cryptocurrencies and commodity futures over the period 2017-2023.

Keywords: Cryptocurrencies, EM algorithm, Generalized Hyperbolic family, Financial networks, Hidden Markov models, Penalized likelihood

1 Introduction

The financial system is a complex, dynamic and interconnected world. Observing the extreme financial integration in the recent global crisis, it was soon noted the crucial importance to identify how the impact of stress events can spread across the whole financial global system. In the last years, the development of statistical techniques to accurately quantify and investigate the interrelations among financial institutions has been at the centre of the attention not only of investors and fund managers, but also of regulators for early identification of systemic risk and proactively engaging preventing measures to control financial stability (Silva et al. 2017, 2018, Giudici & Parisi 2018, Brunetti et al. 2019). For this reason, network science has emerged as a useful tool for describing the propagation of systemic risk, where the interconnectedness between markets is represented by a graph whose nodes stand for companies, commodities, institutions, for instance, and edges represent their interactions. In this context, Gaussian Graphical Models (GGMs) have received an enormous attention because they provide a simple method to model the pair-wise conditional correlations of a collection of stochastic variables. As it is well known, for normally distributed data, the underlying conditional dependence structure is completely characterized by the inverse of the covariance matrix, also known as precision or concentration matrix, of the corresponding GGM (see Lauritzen 1996 for a general background). Thus parameter estimation in GGMs is a fundamental issue for the identification of the zero entries in the concentration matrix. When dealing with large dimensional problems, we are interested in identifying only the variables that exhibit the most relevant and strongest connections. Among the several graphical methods proposed in literature (Dempster 1972, Drton & Perlman 2004, Banerjee et al. 2008, Drton & Perlman 2008, Cai et al. 2011, Liu et al. 2012, Liu & Wang 2017), there exists the popular and computationally efficient *Graphical Lasso* (*lasso*) algorithm of Friedman et al. (2008), which maximizes the likelihood of the model penalized by the L_1 -norm of the elements of the precision matrix.

Moreover, financial time series are characterized by well-known stylized facts like fat tails, leptokurtosis and deviations from normality, that the analysis needs to properly take into account. Especially in the highly turbulent cryptocurrency market, risk managers and regulators are increasingly interested in determining whether, and how, the temporal evolution and volatility clustering of returns can be influenced by hidden variables, e.g., the state of the market, during tranquil and crisis periods. In this context, Hidden Markov Models (HMMs, see MacDonald & Zucchini 1997, Zucchini et al. 2016) have been successfully employed in the analysis of financial time series data, with applications to asset allocation and stock returns as discussed in Mergner & Bulla (2008), De Angelis & Paas (2013), Nystrup et al. (2017), Maruotti et al. (2019), Pennoni et al. (2022) and Feroni et al. (2023a,b). In the context of undirected graphs, estimation of graphical models in HMMs has been addressed by Städler & Mukherjee (2013) using multivariate Gaussian emission distributions with sparse precision matrices which can be interpreted as state-specific conditional independence graphs. More recently, Bianchi et al. (2019) introduced a Markov switching graphical seemingly unrelated regression model to investigate time-varying systemic risk based on a range

of multi-factor asset pricing models. Nevertheless, “non-standard” features of returns cannot be accommodated by standard models such as those based on normality assumptions. Unfortunately, the literature regarding non-Gaussian graphical models is fairly limited. Potential modeling strategies could rely on semiparametric Gaussian copula models (Liu et al. 2012, Xue & Zou 2012), such as the Nonparanormal model of Liu et al. (2009), or power transformations of the data. Alternatively, Finegold & Drton (2011) have introduced a robust graphical model based on the multivariate t distribution called *tlasso*.

In this paper, we contribute to the existing literature by introducing a sparse hidden Markov graphical model to investigate time-varying conditional correlation structures in multivariate time series data, without assuming normally distributed returns. To build our network model, we consider multivariate symmetric generalized hyperbolic (GH, McNeil et al. 2015) distributions with time-dependent parameters evolving according to a discrete, homogeneous latent Markov chain. Within the financial literature, this family of densities has garnered significant attention for describing pertinent features of the distribution of returns (Chen et al. 2008, Necula et al. 2009, Ignatieva & Landsman 2015) but also for its considerable flexibility in modeling financial data (Konlack Socgnia et al. 2014, Zhang et al. 2019) which includes the multivariate Normal, t , Laplace and several others as particular cases (McNeil et al. 2015, Browne & McNicholas 2015). Following Finegold & Drton (2011), we demonstrate that, conditionally on each latent state, the inverse of the state-specific scale matrix of the multivariate GH completely characterizes the conditional correlation structure among the random variables. To induce sparsity in the inverse of the scale matrices, i.e., the precision matrices, and identify whether two nodes are connected by an edge, we exploit the Gaussian location-scale mixture representation of the GH family to build a suitable penalized expectation-conditional maximization either (ECME) algorithm. This enables us to include in our estimation procedure the *glasso* approach of Friedman et al. (2008) accounting for an L_1 penalty on the off-diagonal elements of the precision matrices in the M-step of the algorithm. We call this method *hidden Markov generalized hyperbolic graphical model* (HMGHGM). Within this scheme, our modeling framework allows us to construct a set of regime-specific graphs whose set of edges is determined by the non-zero elements of the estimated state-specific precision matrices. As opposed to GGMs, the proposed methodology has several advantages. Firstly, it enables us to estimate levels of network connectivity among asset returns in different market phases corresponding to different states of the latent process. Secondly, we don’t rely on the restrictive assumption of normally distributed data, but instead each state-dependent GH distribution has shape parameters that are free to vary within the GH family to provide the best fit to the data. Using simulation exercises, we validate the ability of our method to correctly (i) recover the true values of the parameters under different states of the Markov chain, (ii) identify the true HMM clustering partition and (iii) retrieve the graphical model by recovering the true edges of the graphs.

Empirically, we analyze daily returns of a large set of financial assets, including the most important world stock market indices, commodity futures and the largest cryptocurrencies by market capitalization. In the last 10 years, the emergence of the cryptocurrency market has increasingly

attracted the attention of market participants. The shortage of safe assets after the global financial crisis of 2008 has raised several concerns among investors and researchers on whether digital currencies can offer hedging and safe-haven abilities for equity investments (Bouri, Shahzad & Roubaud 2020). In the current literature, there are very few studies examining how traditional asset classes, (i.e., stocks, bonds and exchange rates), commodities and different cryptocurrencies interact with each other. The existing approaches have mainly focused on the relationships between a limited collection of cryptocurrencies and assets (Baur et al. 2018, Corbet et al. 2018, Ji et al. 2018, Bouri, Shahzad, Roubaud, Kristoufek & Lucey 2020, Chen et al. 2020, Giudici & Polinesi 2021) or relied on conditional means to identify correlation structures (Bouri et al. 2017), which cannot provide a complete picture of the dependencies and the transmission path of risks between markets. Here, we implement the proposed HMGHGM to analyze the conditional correlation structure among the cryptocurrency, commodity and stock market sectors from 2017 to 2023 and evaluate how it may vary when considering different volatility clusters. During the period considered, there were significant episodes of prices fluctuations and instability, such as the explosion in cryptocurrencies at the start of 2018, the COVID-19 pandemic erupted in 2020, which have triggered unexpected levels of uncertainty and high volatility, and the EU sanctions to Russia dictated by the Ukrainian war. In this way, we are able to study how the degree of correlation changes as different hidden volatility states are considered.

To the best of our knowledge, this is the first attempt to build a non-gaussian hidden Markov graphical model for estimating time-varying cross-market conditional association structures of financial returns.

The rest of the paper is organized as follows. In Section 2, we briefly review the GH distribution and formally introduce the HMGHGM. Section 3 proposes the ECME-based maximum likelihood approach and the related penalized algorithm for sparse estimation of the state-specific precision matrices. In Section 4 we provide simulation results, while the empirical application is presented in Section 5. Section 6 summarizes our conclusions.

2 Methodology

In this section we introduce the hidden Markov generalized hyperbolic graphical model (HMGHGM). Before describing the model, we briefly revise the symmetric multivariate GH distribution, its location-scale mixture representation and its limiting cases. Subsequently, we show how it is possible to build sparse state-specific graphical models for characterizing time-varying conditional correlation relations among variables.

2.1 The generalized hyperbolic distribution and its special cases

Formally, let $\mathbf{Y}_t = [Y_t^{(1)}, \dots, Y_t^{(d)}]'$ denote a continuous d -dimensional random vector for $t = 1, \dots, T$. The joint probability density function of \mathbf{Y}_t following the (symmetric) GH distribution can be written as

$$f_{\mathbf{Y}_t}(\mathbf{y}_t; \boldsymbol{\mu}, \boldsymbol{\Sigma}, \lambda, \chi, \psi) = \frac{1}{(2\pi)^{d/2} |\boldsymbol{\Sigma}|^{1/2} K_\lambda(\sqrt{\psi\chi})} \left[\frac{\chi + \delta(\mathbf{y}_t; \boldsymbol{\mu}, \boldsymbol{\Sigma})}{\psi} \right]^{\frac{\lambda-d/2}{2}} K_{\lambda-\frac{d}{2}} \left(\sqrt{[\chi + \delta(\mathbf{y}_t; \boldsymbol{\mu}, \boldsymbol{\Sigma})] \psi} \right) \quad (1)$$

where $\boldsymbol{\mu} \in \mathbb{R}^d$ is the location parameter, $\boldsymbol{\Sigma}$ is a $d \times d$ positive definite and symmetric scale matrix, such that $|\boldsymbol{\Sigma}| = 1$ for identifiability purposes (see [McNeil et al. \(2015\)](#) for details), $\lambda \in \mathbb{R}$ is the index parameter, $\chi > 0$ and $\psi > 0$ are concentration parameters, $\delta(\mathbf{y}_t; \boldsymbol{\mu}, \boldsymbol{\Sigma}) = (\mathbf{y}_t - \boldsymbol{\mu})' \boldsymbol{\Sigma}^{-1} (\mathbf{y}_t - \boldsymbol{\mu})$ is the squared Mahalanobis distance between \mathbf{y}_t and $\boldsymbol{\mu}$ with scale matrix $\boldsymbol{\Sigma}$ and finally $K_{\lambda-\frac{d}{2}}(\cdot)$ denotes the modified Bessel function of the third kind of order $\lambda - \frac{d}{2}$. We adopt the compact notation $\mathbf{Y}_t \sim \mathcal{GH}_d(\boldsymbol{\mu}, \boldsymbol{\Sigma}, \lambda, \chi, \psi)$. One of the key benefits of the GH distribution is that, using (1), \mathbf{Y}_t admits the following location-scale mixture representation:

$$\mathbf{Y}_t = \boldsymbol{\mu} + \sqrt{W_t} \boldsymbol{\Sigma}^{1/2} \mathbf{Z}_t \quad (2)$$

where $\mathbf{Z}_t \sim \mathcal{N}_d(\mathbf{0}_d, \mathbf{I}_d)$ denotes a d -variate standard Normal distribution whose covariance matrix is the identity matrix and W_t has a generalized inverse Gaussian (GIG) distribution, $W_t \sim \mathcal{GIG}(\lambda, \chi, \psi)$, with \mathbf{Z}_t being independent of W_t . From (2), we can refer to the following hierarchical representation of $\mathbf{Y}_t \sim \mathcal{GH}_d(\boldsymbol{\mu}, \boldsymbol{\Sigma}, \lambda, \chi, \psi)$:

$$\begin{aligned} W_t &\sim \mathcal{GIG}(\lambda, \chi, \psi), \\ \mathbf{Y}_t | W_t = w_t &\sim \mathcal{N}_d(\boldsymbol{\mu}, w_t \boldsymbol{\Sigma}) \end{aligned} \quad (3)$$

which is useful for random data generation and for the implementation of our ECME algorithm.

The GH family encompasses several well-known, applied models for financial data by varying appropriately the values of the parameters of the GIG distribution, (λ, χ, ψ) , including the multivariate Laplace, t and Normal distribution as presented in [Figure 1](#).

A complete taxonomy of all the models belonging to the class of GH densities can be found, for instance, in [McNeil et al. \(2015\)](#), [Browne & McNicholas \(2015\)](#) and [Bagnato et al. \(2023\)](#).

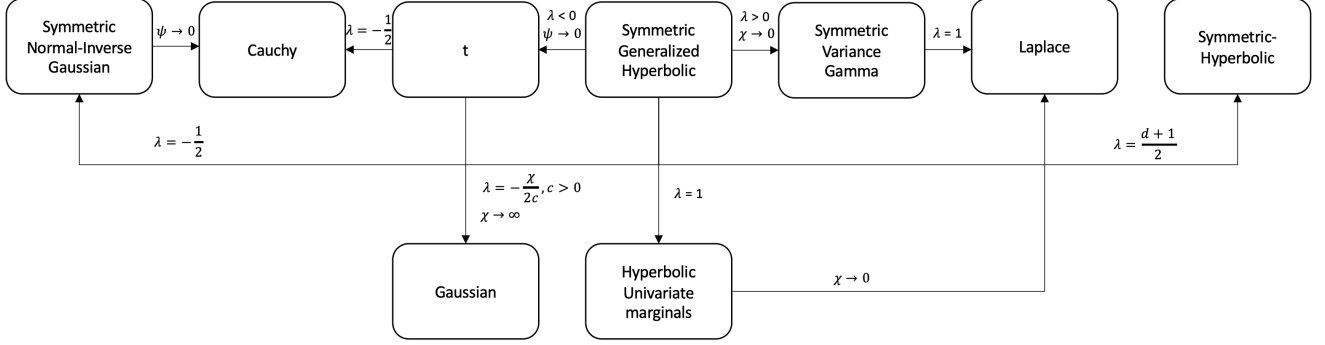


Figure 1: Special and limiting cases of the symmetric GH distribution in terms of λ , χ and ψ .

2.2 Hidden Markov graphical models with state-specific GH densities

In this section we describe the proposed hidden Markov graphical model with state-specific multivariate GH emission densities.

Formally, let $\{S_t\}_{t=1}^T$ be a latent, homogeneous, first-order Markov chain defined on the discrete state space $\{1, \dots, K\}$. Let $\pi_k = Pr(S_1 = k)$ be the initial probability of state k , $k = 1, \dots, K$, and $\pi_{k|j} = Pr(S_{t+1} = k | S_t = j)$, with $\sum_{k=1}^K \pi_{k|j} = 1$ and $\pi_{k|j} \geq 0$, denote the transition probability between states j and k , that is, the probability to visit state k at time $t + 1$ from state j at time t , $j, k = 1, \dots, K$ and $t = 1, \dots, T$. We collect the initial and transition probabilities in the K -dimensional vector $\boldsymbol{\pi}$ and in the $K \times K$ matrix $\boldsymbol{\Pi}$, respectively.

In our model we assume that the conditional distribution of \mathbf{Y}_t given the state occupied by the latent process at time t corresponds to a GH distribution in (1) whose parameters depend on the value of the Markov chain S_t , namely $\mathbf{Y}_t | S_t = k \sim \mathcal{GH}_d(\boldsymbol{\mu}_k, \boldsymbol{\Sigma}_k, \lambda_k, \chi_k, \psi_k)$. We define with $\boldsymbol{\Theta}_k = \boldsymbol{\Sigma}_k^{-1}$ for $k = 1, \dots, K$, the precision matrices used to build state-specific undirected graphs that conveys the conditional intercorrelation structure among the elements of \mathbf{Y}_t given the latent process S_t . More precisely, supposing $S_t = k$, let $G_k = (V, E_k)$ be an undirected state-dependent graph where $V = \{1, \dots, d\}$ denotes the set of state-invariant nodes, such that each component of the random variable \mathbf{Y}_t corresponds to a node in V , and $E_k \subseteq V \times V$ represents the set of undirected edges in the k -th state. In order to study the conditional correlation structure of \mathbf{Y}_t within the k -th state through the graph G_k , we establish a useful result that allows us to make inference on the edge set E_k based on the precision matrix $\boldsymbol{\Theta}_k$. Following [Finegold & Drton \(2011\)](#) and exploiting the mixture representation of the symmetric GH in (2), we can characterize the conditional correlation structure as shown in the following proposition.

Proposition 1. *Consider $S_t = k$ and let $\mathbf{Y}_t | S_t = k \sim \mathcal{GH}_d(\boldsymbol{\mu}_k, \boldsymbol{\Sigma}_k, \lambda_k, \chi_k, \psi_k)$. If two nodes j and h , with $j, h \in V$ and $j \neq h$, of the graph are separated by a set of nodes $C \in V$, then $Y_t^{(j)}$ and $Y_t^{(h)}$ are conditionally uncorrelated given $\mathbf{Y}_t^{(C)}$ and $S_t = k$.*

Proof. Without loss of generality, throughout the proof we omit the subscript k indicating the latent state yet all the following equalities are conditional on $S_t = k$. To prove the result it is

sufficient to show that $Y_t^{(j)}$ and $Y_t^{(h)}$ are conditionally uncorrelated given $\mathbf{Y}_t^{(V \setminus \{j, h\})}$. Partition V into $a = \{j, h\}$ and $b = V / \{j, h\}$. For a given value of W_t and given $\Theta = \Sigma^{-1}$:

$$(\mathbf{Y}_t^{(a)} | \mathbf{Y}_t^{(b)}, W_t) \sim \mathcal{N}_2(\boldsymbol{\mu}^{(a)} - \Theta_{a,a}^{-1} \Theta_{a,b} (\mathbf{Y}_t^{(b)} - \boldsymbol{\mu}^{(b)}), W_t \Theta_{a,a}^{-1}) \quad (4)$$

and

$$(Y_t^{(j)} | \mathbf{Y}_t^{(h \cup b)}, W_t) \sim \mathcal{N}_1(\mu^{(j)} - \Theta_{j,j}^{-1} \Theta_{j, h \cup b} (\mathbf{Y}_t^{(h \cup b)} - \boldsymbol{\mu}^{(h \cup b)}), W_t \Theta_{j,j}^{-1}), \quad (5)$$

where $\Theta_{a,b}$ is the submatrix of Θ with rows and columns indexed by the sets a and b . Since $\Theta_{j,h} = 0$,

$$\begin{aligned} E[Y_t^{(j)} | \mathbf{Y}_t^{(h \cup b)}, W_t] &= \mu^{(j)} - \Theta_{j,j}^{-1} \Theta_{j,b} (\mathbf{Y}_t^{(b)} - \boldsymbol{\mu}^{(b)}) \\ &= E[Y_t^{(j)} | \mathbf{Y}_t^{(b)}, W_t] \end{aligned} \quad (6)$$

for any value of W_t . Therefore,

$$\begin{aligned} E[Y_t^{(j)} | \mathbf{Y}_t^{(h \cup b)}] &= E[E[Y_t^{(j)} | \mathbf{Y}_t^{(h \cup b)}, W_t] | \mathbf{Y}_t^{(h \cup b)}] = E[E[Y_t^{(j)} | \mathbf{Y}_t^{(b)}, W_t] | \mathbf{Y}_t^{(b)}] \\ &= E[Y_t^{(j)} | \mathbf{Y}_t^{(b)}] \end{aligned} \quad (7)$$

which implies that $Y_t^{(j)}$ and $Y_t^{(h)}$ are conditionally uncorrelated given $\mathbf{Y}_t^{(b)}$. \square

Based on (4), we can exploit the properties of GGMs to characterize conditional correlation relationships between the elements of \mathbf{Y}_t in each state $k = 1, \dots, K$, estimating the precision matrices Θ_k 's. More formally, for each state and for any pair of nodes j, h , with $j \neq h$, $Y_t^{(j)}$ and $Y_t^{(h)}$ are conditionally uncorrelated given $\mathbf{Y}_t^{(V \setminus \{j, h\})}$ and $S_t = k$ if and only if the (j, h) -th element of the matrix Θ_k , $\Theta_{k,j,h}$, is equal to 0. Hence, for each $k = 1, \dots, K$, the edge set E_k of the graph G_k describing the distribution of $\mathbf{Y}_t | S_t = k$ is completely encoded by the matrix Θ_k of the GH distribution, i.e., $(j, h) \in E_k$ if and only if $\Theta_{k,j,h} \neq 0$. The proposed methodology allows us to capture regime-specific conditional correlation structures for probability distributions within the GH family. With respect to alternative strategies, our framework is a generalization of the graphical model of [Finegold & Drton \(2011\)](#) when $K = 1$ where the GH reduces to the multivariate t distribution. In addition, we encompass the graphical hidden Markov model of [Städler & Mukherjee \(2013\)](#) when the state-specific GH emission densities reduce to the multivariate Normal distributions.

In this setting, it is therefore crucial to accurately determine the matrices $\Theta_1, \dots, \Theta_K$ for a correct interpretation of the graphs and to visualize the true interactions among the variables. In section 3, we introduce a maximum likelihood approach to estimate the model parameters and make inference on the sparsity pattern in the Θ_k 's.

3 Estimation

As shown in the previous sections, the location-scale mixture representation of the GH is a convenient tool to build a sparse graphical model. As is common for HMMs, and for latent variable models in general, we propose a suitable likelihood-based EM algorithm (Baum et al. 1970) to estimate the parameters of the method proposed based on the observed data. Since we are interested in detecting only the most important connections, we also propose a penalized version of the EM by considering the Lasso-type regularization of Tibshirani (1996) for sparse matrix estimation in high-dimensional settings where a large number of variables is available.

3.1 The EM algorithm

For a given number of hidden states K , the EM algorithm runs on the complete log-likelihood function of the model introduced, which is defined as

$$\begin{aligned} \ell_c(\boldsymbol{\theta}) = & \sum_{k=1}^K \gamma_1(k) \log \pi_k + \sum_{t=1}^T \sum_{k=1}^K \sum_{j=1}^K \xi_t(j, k) \log \pi_{k|j} \\ & + \sum_{t=1}^T \sum_{k=1}^K \gamma_t(k) \log f_Y(\mathbf{y}_t | S_t = k), \end{aligned} \quad (8)$$

where $\boldsymbol{\theta} = (\boldsymbol{\mu}_1, \dots, \boldsymbol{\mu}_K, \boldsymbol{\Sigma}_1, \dots, \boldsymbol{\Sigma}_K, \lambda_1, \dots, \lambda_K, \psi_1, \dots, \psi_K, \chi_1, \dots, \chi_K, \boldsymbol{\pi}, \mathbf{\Pi})$ represents the vector of all model parameters, $\gamma_t(k)$ denotes a dummy variable equal to 1 if the latent process is in state k at occasion t and 0 otherwise, and $\xi_t(j, k)$ is a dummy variable equal to 1 if the process is in state j in $t - 1$ and in state k at time t and 0 otherwise.

Unfortunately, the log-likelihood of the GH distribution does not yield any closed-form expression in the optimization process. Nevertheless, following Chatzis (2010), the issue can be resolved exploiting the data augmentation scheme of equation (3). We exploit the conditional structure by writing

$$\log f_Y(\mathbf{y}_t | S_t = k) = l_1(\boldsymbol{\mu}_k, \boldsymbol{\Sigma}_k | S_t = k) + l_2(\lambda_k, \chi_k, \psi_k | S_t = k) \quad (9)$$

where

$$l_1(\boldsymbol{\mu}_k, \boldsymbol{\Sigma}_k | S_t = k) = \sum_{t=1}^T \left[-\frac{d}{2} \log(2\pi) - \frac{d}{2} \log(w_{tk}) - \frac{1}{2} \log |\boldsymbol{\Sigma}_k| - \frac{\delta(\mathbf{y}_t; \boldsymbol{\mu}_k, \boldsymbol{\Sigma}_k)}{2w_{tk}} \right] \quad (10)$$

and

$$l_2(\lambda_k, \chi_k, \psi_k | S_t = k) = \sum_{t=1}^T \left\{ (\lambda_k - 1) \log(w_{tk}) - \frac{1}{2} \frac{\chi_k}{w_{tk}} - \frac{1}{2} \psi_k w_{tk} - \frac{1}{2} \lambda_k \log(\chi_k) + \frac{1}{2} \lambda_k \log(\psi_k) - \log \left[2K_{\lambda_k} \left(\sqrt{(\psi_k \chi_k)} \right) \right] \right\} \quad (11)$$

Working on $\ell_c(\boldsymbol{\theta})$, we adopt the expectation-conditional maximization either (ECME) algorithm of Liu & Rubin (1994). The ECME algorithm is an extension of the expectation-conditional

maximum (ECM) algorithm which replaces the M-step of the EM algorithm by a number of computationally simpler conditional maximization (CM) steps. The ECME algorithm generalizes the ECM one by conditionally maximizing on some or all of the CM-steps the incomplete-data log-likelihood. In our case, the ECME algorithm iterates between four steps, one E-step and three CM-steps, until convergence. The three CM-steps arise from the update of the partition of $\boldsymbol{\theta}$ as $\{\boldsymbol{\theta}_1, \boldsymbol{\theta}_2, \boldsymbol{\theta}_3\}$, where $\boldsymbol{\theta}_1 = \{\boldsymbol{\mu}_1, \boldsymbol{\Sigma}_1, \dots, \boldsymbol{\mu}_K, \boldsymbol{\Sigma}_K\}$, $\boldsymbol{\theta}_2 = \{\lambda_1, \chi_1, \psi_1, \dots, \lambda_K, \chi_K, \psi_K\}$ and $\boldsymbol{\theta}_3 = \{\boldsymbol{\pi}, \boldsymbol{\Pi}\}$.

E-step:

In the E-step, at the generic $(h + 1)$ -th iteration, the unobservable indicator variables $\gamma_t(k)$ and $\xi_t(j, k)$ in (8) are replaced by their conditional expectations given the observed data and the current parameter estimates $\boldsymbol{\theta}^{(h)}$. To compute such quantities we require the calculation of the probability of being in state k at time t given the observed sequence

$$\gamma_t^{(h)}(k) = P_{\boldsymbol{\theta}^{(h)}}(S_t = k | \mathbf{y}_1, \dots, \mathbf{y}_T) \quad (12)$$

and the probability that at time $t - 1$ the process is in state j and then in state k at time t , given the observed sequence

$$\xi_t^{(h)}(j, k) = P_{\boldsymbol{\theta}^{(h)}}(S_{t-1} = j, S_t = k | \mathbf{y}_1, \dots, \mathbf{y}_T). \quad (13)$$

The quantities in (12) and (13) can be obtained using the Forward-Backward algorithm of [Welch \(2003\)](#).

Then, we use these to calculate the conditional expectation of (8), given the observed data and the current estimates:

$$\begin{aligned} Q(\boldsymbol{\theta} | \boldsymbol{\theta}^{(h)}) &= \sum_{k=1}^K \gamma_1^{(h)}(k) \log \pi_k + \sum_{t=1}^T \sum_{k=1}^K \sum_{j=1}^K \xi_t^{(h)}(j, k) \log \pi_{k|j} \\ &+ \sum_{t=1}^T \sum_{k=1}^K \gamma_t^{(h)}(k) \left[Q_1(\boldsymbol{\mu}_k, \boldsymbol{\Sigma}_k | \boldsymbol{\theta}^{(h)}, S_t = k) + Q_2(\lambda_k, \chi_k, \psi_k | \boldsymbol{\theta}^{(h)}, S_t = k) \right]. \end{aligned} \quad (14)$$

In (14), $Q_1(\boldsymbol{\mu}_k, \boldsymbol{\Sigma}_k | \boldsymbol{\theta}^{(h)}, S_t = k)$ and $Q_2(\lambda_k, \chi_k, \psi_k | \boldsymbol{\theta}^{(h)}, S_t = k)$ are respectively the conditional expectations of $l_1(\boldsymbol{\mu}_k, \boldsymbol{\Sigma}_k | S_t = k)$ and $l_2(\lambda_k, \chi_k, \psi_k | S_t = k)$ given the observed data, using the current $\boldsymbol{\theta}^{(h)}$ for $\boldsymbol{\theta}$. To compute Q_1 and Q_2 , we have to consider the expected value of any function of the latent variable W_{tk} in equation (10). In particular the functions are w_{tk} , $1/w_{tk}$ and $\log(w_{tk})$ and their expected values must be calculated with respect to the current $\boldsymbol{\theta}^{(h)}$. Since the conditional distribution of W_{tk} given \mathbf{Y}_t corresponds to a GIG distribution with parameters $\lambda_k - \frac{d}{2}, \delta(\mathbf{y}_t; \boldsymbol{\mu}_k, \boldsymbol{\Sigma}_k) + \chi_k, \psi_k$, i.e.,

$$f_{W_{tk} | \mathbf{Y}_t}(w_{tk} | \mathbf{Y}_t = \mathbf{y}_t, S_t = k) \sim GIG(\lambda_k - \frac{d}{2}, \delta(\mathbf{y}_t; \boldsymbol{\mu}_k, \boldsymbol{\Sigma}_k) + \chi_k, \psi_k), \quad (15)$$

it follows that (see [Chatzis 2010](#))

$$v_{tk}^{(h)} = E^{(h)}[W_{tk} | \mathbf{Y}_t = \mathbf{y}_t, S_t = k] = \left(\frac{\delta(\mathbf{y}_t; \boldsymbol{\mu}_k^{(h)}, \boldsymbol{\Sigma}_k^{(h)}) + \chi_k^{(h)}}{\psi_k^{(h)}} \right)^{\frac{1}{2}} \frac{K_{\lambda_k^{(h)} - \frac{d}{2} + 1} \left(\sqrt{\psi_k^{(h)} \left[\delta(\mathbf{y}_t; \boldsymbol{\mu}_k^{(h)}, \boldsymbol{\Sigma}_k^{(h)}) + \chi_k^{(h)} \right]} \right)}{K_{\lambda_k^{(h)} - \frac{d}{2}} \left(\sqrt{\psi_k^{(h)} \left[\delta(\mathbf{y}_t; \boldsymbol{\mu}_k^{(h)}, \boldsymbol{\Sigma}_k^{(h)}) + \chi_k^{(h)} \right]} \right)}, \quad (16)$$

$$u_{tk}^{(h)} = E^{(h)}[W_{tk}^{-1} | \mathbf{Y}_t = \mathbf{y}_t, S_t = k] = \left(\frac{\delta(\mathbf{y}_t; \boldsymbol{\mu}_k^{(h)}, \boldsymbol{\Sigma}_k^{(h)}) + \chi_k^{(h)}}{\psi_k^{(h)}} \right)^{-\frac{1}{2}} \frac{K_{\lambda_k^{(h)} - \frac{d}{2} + 1} \left(\sqrt{\psi_k^{(h)} \left[\delta(\mathbf{y}_t; \boldsymbol{\mu}_k^{(h)}, \boldsymbol{\Sigma}_k^{(h)}) + \chi_k^{(h)} \right]} \right)}{K_{\lambda_k^{(h)} - \frac{d}{2}} \left(\sqrt{\psi_k^{(h)} \left[\delta(\mathbf{y}_t; \boldsymbol{\mu}_k^{(h)}, \boldsymbol{\Sigma}_k^{(h)}) + \chi_k^{(h)} \right]} \right)} - \frac{2 \left(\lambda_k^{(h)} - \frac{d}{2} \right)}{\delta(\mathbf{y}_t; \boldsymbol{\mu}_k^{(h)}, \boldsymbol{\Sigma}_k^{(h)}) + \chi_k^{(h)}} \quad (17)$$

and

$$z_{tk}^{(h)} = E^{(h)}[\log(W_{tk}) | \mathbf{Y}_t = \mathbf{y}_t, S_t = k] = \log \left(\sqrt{\frac{\delta(\mathbf{y}_t; \boldsymbol{\mu}_k^{(h)}, \boldsymbol{\Sigma}_k^{(h)}) + \chi_k^{(h)}}{\psi_k^{(h)}}} \right) + \frac{\partial}{\partial \lambda_k^{(h)}} \log K_{\lambda_k^{(h)} - \frac{d}{2}} \left(\sqrt{\psi_k^{(h)} \left[\delta(\mathbf{y}_t; \boldsymbol{\mu}_k^{(h)}, \boldsymbol{\Sigma}_k^{(h)}) + \chi_k^{(h)} \right]} \right). \quad (18)$$

As a consequence, substituting w_{tk} , $1/w_{tk}$ and $\log(w_{tk})$ with $v_{tk}^{(h)}$, $u_{tk}^{(h)}$ and $z_{tk}^{(h)}$ respectively in $l_1(\boldsymbol{\mu}_k, \boldsymbol{\Sigma}_k | S_t = k)$ and $l_2(\lambda_k, \chi_k, \psi_k | S_t = k)$ we obtain

$$Q_1(\boldsymbol{\mu}_l, \boldsymbol{\Sigma}_k | \boldsymbol{\theta}^{(h)}, S_t = k) = \sum_{t=1}^T \left[-\frac{1}{2} \log |\boldsymbol{\Sigma}_k| - \frac{u_{tk}^{(h)} \delta(\mathbf{y}_t; \boldsymbol{\mu}_k, \boldsymbol{\Sigma}_k)}{2} \right] \quad (19)$$

$$Q_2(\lambda_k, \chi_k, \psi_k | \boldsymbol{\theta}^{(h)}, S_t = k) = \sum_{t=1}^T \left\{ (\lambda_k - 1) z_{tk}^{(h)} - u_{tk}^{(h)} \frac{\chi_k}{2} - \frac{\psi_k}{2} v_{tk}^{(h)} - \frac{\lambda_k}{2} [\log(\chi_k) + \log(\psi_k)] - \log \left[2K_{\lambda_k} \left(\sqrt{\psi_k \chi_k} \right) \right] \right\} \quad (20)$$

where in (19) we dropped the terms which are constant with respect to $\boldsymbol{\mu}_k$ and $\boldsymbol{\Sigma}_k$.

CM-step 1:

The initial probabilities π_k and transition probabilities $\pi_{k|j}$ of the partition $\boldsymbol{\theta}_3$ are updated using:

$$\pi_k^{(h+1)} = \gamma_1^{(h)}(k), \quad k = 1, \dots, K \quad (21)$$

and

$$\pi_{k|j}^{(h+1)} = \frac{\sum_{t=1}^T \xi_t^{(h)}(j, k)}{\sum_{t=1}^T \sum_{k=1}^K \xi_t^{(h)}(j, k)}, \quad j, k = 1, \dots, K. \quad (22)$$

CM-step 2:

The second maximization step requires the calculation of $\boldsymbol{\theta}_1^{(h+1)}$ as the value of $\boldsymbol{\theta}_1$ that maximizes $Q_1(\boldsymbol{\mu}_k, \boldsymbol{\Sigma}_k | \boldsymbol{\theta}^{(h)}, S_t = k)$ in (19), with $\boldsymbol{\theta}_2$ fixed at $\boldsymbol{\theta}_2^{(h+1)}$. The first order conditions with respect to $\boldsymbol{\mu}_k$ and $\boldsymbol{\Theta}_k = \boldsymbol{\Sigma}_k^{-1}$ yield

$$\frac{\partial Q_1(\boldsymbol{\mu}_k, \boldsymbol{\Sigma}_k | \boldsymbol{\theta}_2^{(h)})}{\partial \boldsymbol{\mu}_k} = \sum_{t=1}^T \sum_{k=1}^K u_{tk}^{(h)} (\mathbf{y}_t - \boldsymbol{\mu}_k) \gamma_t^{(h)}(k) \quad (23)$$

$$\frac{\partial Q_1(\boldsymbol{\mu}_k, \boldsymbol{\Theta}_k | \boldsymbol{\theta}_2^{(h)})}{\partial \boldsymbol{\Theta}_k} = \sum_{t=1}^T \sum_{k=1}^K \gamma_t^{(h)}(k) \left[\frac{1}{2} \frac{\partial}{\partial \boldsymbol{\Theta}_k} \log |\boldsymbol{\Theta}_k| - \frac{1}{2} u_{tk}^{(h)} \frac{\partial}{\partial \boldsymbol{\Theta}_k} (\mathbf{y}_t - \boldsymbol{\mu}_k)' \boldsymbol{\Theta}_k (\mathbf{y}_t - \boldsymbol{\mu}_k) \right] \quad (24)$$

so the CM-step update expressions for $\boldsymbol{\mu}_k$ and $\boldsymbol{\Sigma}_k$ are

$$\boldsymbol{\mu}_k^{(h+1)} = \frac{\sum_{t=1}^T \sum_{k=1}^K \gamma_t^{(h)}(k) u_{tk}^{(h)} \mathbf{y}_t}{\sum_{t=1}^T \sum_{k=1}^K \gamma_t^{(h)}(k) u_{tk}^{(h)}} \quad (25)$$

and

$$\boldsymbol{\Sigma}_k^{(h+1)} = |\boldsymbol{\Sigma}_k^{*(h+1)}|^{-\frac{1}{d}} \boldsymbol{\Sigma}_k^{*(h+1)} \quad (26)$$

where

$$\boldsymbol{\Sigma}_k^{*(h+1)} = \frac{\sum_{t=1}^T \sum_{k=1}^K \gamma_t^{(h)}(k) u_{tk}^{(h)} (\mathbf{y}_t - \boldsymbol{\mu}_k^{(h+1)})' (\mathbf{y}_t - \boldsymbol{\mu}_k^{(h+1)})}{\sum_{t=1}^T \sum_{k=1}^K \gamma_t^{(h)}(k)} \quad (27)$$

In (26), the scalar $|\boldsymbol{\Sigma}_k^{*(h+1)}|^{-\frac{1}{d}}$ is needed to ensure the identifiability constraint $|\boldsymbol{\Sigma}_k^{(h+1)}| = 1$.

CM-step 3:

In the third CM-step we choose the value of $\boldsymbol{\theta}_2$ that maximizes $\ell_c(\boldsymbol{\theta})$ in (8), with $\boldsymbol{\theta}_1$ fixed at $\boldsymbol{\theta}_1^{(h+1)}$. As a closed-form solution for $\boldsymbol{\theta}_2^{(h+1)}$ is not analytically available, numerical optimization can be used with this aim. As in [Bagnato et al. \(2023\)](#), we perform an unconstrained maximization on \mathbb{R}^3 , based on a (log/exp) transformation/back-transformation approach for χ_k and ψ_k .

The E- and CM-steps are alternated until convergence, that is when the observed likelihood between two consecutive iterations is smaller than a predetermined threshold. In this paper, we set this threshold criterion equal to 10^{-8} .

For fixed K we initialize the ECME algorithm by providing the initial states partition, $\{S_t^{(0)}\}_{t=1}^T$, according to the K -means algorithm. From the generated partition, the elements of $\boldsymbol{\Pi}^{(0)}$ are computed as proportions of transition. The location parameters $\boldsymbol{\mu}_1, \dots, \boldsymbol{\mu}_K$ are obtained from the centroid of the the derived clusters while we set the initial values of the $\boldsymbol{\Sigma}_k$'s as the empirical covariance matrices of the obtained clusters with unit determinant using (26). Finally, the

$(\lambda_k, \chi_k, \psi_k)$'s are initialized from uniform distributions. To deal with the possibility of multiple roots of the likelihood equation and better explore the parameter space, we fit the proposed HMGHGM using a multiple random starts strategy with different starting partitions and retain the solution corresponding to the maximum likelihood value.

All the computations have been conducted using the R software, version 4.3.0 (R Core Team 2023).

3.2 Penalized inference with the GH distribution

In this section we extend the procedure described above for estimating high-dimensional graphs where the number of model parameters grows with the dimension of the problem. Indeed, the correct identification of the sparsity patterns is a fundamental issue for capturing the most relevant interconnections, which motivates us to use sparse estimators that automatically shrink the elements of the inverse of the scale matrix matrix. In the literature, within the GGMs context, several works have been put forward to obtain sparse estimates of the concentration matrix. Friedman et al. (2008) introduced the efficient coordinate descent algorithm, denoted as *glasso*, to estimate a sparse graph using the Lasso L_1 penalty of Tibshirani (1996). Gao & Massam (2015) proposed to estimate the concentration matrix using further penalties, i.e., the smoothly clipped absolute deviation of Fan & Li (2001) and the minimax concave penalty of Zhang et al. (2010). Alternatively Meinshausen & Bühlmann (2006) presented a neighbourhood selection scheme that estimates the conditional independence relations separately for each node in the graph by using L_1 -penalized regressions.

In this work, we exploit the efficient *glasso* approach of Friedman et al. (2008) to induce sparsity in the precision matrices of the GH for each latent state, without relying on the limitation of normally distributed returns. Specifically, starting from the EM algorithm of Section 3 and following Green (1990), we construct a PEM algorithm by adding to the complete likelihood in (8) an L_1 -norm penalty that shrinks to zero the off-diagonal elements of the Θ_k^{-1} 's. The penalized version of the conditional Normal log-likelihood in (10) is reported in the following definition.

Definition 1. The conditional Normal log-likelihood function is proportional to:

$$\ell_{1,pen}(\boldsymbol{\mu}_k, \Theta_k | \mathbf{Y}_t, W_{tk}, S_t = k) \propto \frac{1}{2} \sum_{t=1}^T \gamma_t(k) \log |\Theta_k| - \frac{1}{2} \text{tr}\{\tilde{\mathbf{S}}_k \Theta_k\} - \rho \sqrt{\nu_k} \|\Theta_k\|_1 \quad (28)$$

where $\|\Theta_k\|_1$ is the sum of the absolute values of the off-diagonal entries of the matrix Θ_k and $\tilde{\mathbf{S}}_k$ is the weighted empirical covariance matrix defined as

$$\tilde{\mathbf{S}}_k = \sum_{t=1}^T \frac{\gamma_t(k)}{W_{tk}} (\mathbf{Y}_t - \boldsymbol{\mu}_k)(\mathbf{Y}_t - \boldsymbol{\mu}_k)'. \quad (29)$$

Additionally, $\nu_k > 0$ is a state-dependent weight to allow for a different penalty in each latent state such that $\sum_{k=1}^K \nu_k = 1$ and $\rho \geq 0$ is the tuning parameter.

As one can see, the penalized complete likelihood in (28) is exactly the objective function maximized in a GGM where the empirical covariance matrix of the data is substituted by the matrix $\tilde{\mathbf{S}}_k$ defined in (29), for $k = 1, \dots, K$. This suggests that we can exploit the simple and fast *glasso* algorithm of [Friedman et al. \(2008\)](#) to update the estimate of Θ_k . More specifically, for a given value of ρ , the proposed PEM alternates between the E-step described in Section 3.1 and essentially modifies the CM-step 2 by maximizing the quantity in (28).

4 Simulation study

We conduct a simulation study to validate the performance of our model under different scenarios in terms of:

1. recovering the true values of the parameters for a varying number of hidden states,
2. clustering performance,
3. the ability to correctly retrieve the edge sets associated to each hidden state.

Scenario 1: In the first scenario we consider a 2-dimensional vector \mathbf{Y}_t with sample size of $T = 1000$, 150 Monte Carlo simulations, 70 random starts for the EM algorithm and we draw observations from a one-, two- and three-state HMM. Conditional on the hidden state, observations are generated from the following six models: Gaussian, t, Cauchy, Laplace, generalized hyperbolic and variance gamma (see Table 1). They all share the same location and scale parameters $\boldsymbol{\mu}_1 = [5, 5]$, $\boldsymbol{\Sigma}_1 = [1.51, -1.13, -1.13, 1.51]$, $\boldsymbol{\mu}_2 = [-5, -5]$, $\boldsymbol{\Sigma}_2 = [1.51, 1.13, 1.13, 1.51]$, $\boldsymbol{\mu}_3 = [0, 0]$, $\boldsymbol{\Sigma}_3 = [1.01, .12, .12, 1.01]$. Parameters λ , χ , ψ are state-invariant and they are chosen so to obtain the six models in Table 1. In this first scenario, to fit the proposed model we use the non penalized ECME algorithm discussed in Section 3.1. The matrices of transition probabilities and the vectors of initial probabilities are set equal to $\boldsymbol{\Pi} = \begin{pmatrix} 0.9 & 0.1 \\ 0.1 & 0.9 \end{pmatrix}$ and $\boldsymbol{\pi} = [0.7, 0.3]$ for $K = 2$, and to $\boldsymbol{\Pi} = \begin{pmatrix} 0.8 & 0.1 & 0.1 \\ 0.1 & 0.8 & 0.1 \\ 0.1 & 0.1 & 0.8 \end{pmatrix}$ and $\boldsymbol{\pi} = [0.4, 0.3, 0.3]$ for $K = 3$, respectively. In order to assess the validity of our model we compute the point estimate and standard error values associated to the state-specific coefficients, averaged over the Monte Carlo replications. Tables 2, 3, 5, 4, 6, 7 illustrate the results for the six data generating models considered. For every model, the estimated location and scale parameters are very close to the true values. This is also true for the parameters $(\lambda_k, \chi_k, \psi_k)$ in every state. In particular, for the Gaussian generating model where λ_k is constrained so that $\lambda_k = -\chi_k/2$, we observe large values for χ_k whereas ψ_k is approximately zero. For all the other distributions, the point estimates of λ_k are always very close to the real values in Table 1. The estimated ψ_k 's are small for the t and the Cauchy, while, as expected, are very close to 0.5 for the Cauchy and variance gamma. Finally, as regards the χ_k 's, they are close to 2 for the t, the Cauchy and the Generalized Hyperbolic, and near to zero for the Laplace and variance gamma.

Scenario 2: To evaluate the ability in recovering the true states partition we consider the Adjusted Rand Index (ARI) of [Hubert & Arabie \(1985\)](#). The state partition provided by the fitted models

Parameters	Gaussian	t	Cauchy	Laplace	generalized hyperbolic	variance gamma
λ	-20	-1	-0.5	1	$(d+1)/2$	1.5
χ	40	2	2	0.001	2	0.001
ψ	0.001	0.001	0.001	0.5	3	0.5

Table 1: Values of the parameters λ , χ , ψ used in the simulation study.

	$\boldsymbol{\mu}_k$		$\boldsymbol{\Sigma}_k$				λ	χ	ψ
<i>K</i> = 1									
Est.	4.982	5.008	1.506	-1.123	-1.123	1.507	-8.261	16.522	0.139
Std. Err.	0.061	0.054	0.05	0.053	0.053	0.051	1.514	3.027	0.059
<i>K</i> = 2									
Est.	-4.99	-4.984	1.5	-1.119	-1.119	1.502	-7.472	14.945	0.038
Std. Err.	0.086	0.079	0.072	0.075	0.075	0.078	6.828	13.656	0.134
Est.	4.987	5.007	1.527	1.147	1.147	1.517	-11.16	22.321	0.002
Std. Err.	0.086	0.09	0.074	0.071	0.071	0.072	5.827	11.655	0.135
<i>K</i> = 3									
Est.	-5.102	-5.098	1.51	-1.137	-1.137	1.518	-7.961	15.922	0.003
Std. Err.	0.142	0.133	0.086	0.095	0.095	0.096	6.255	12.509	0.091
Est.	-0.02	-0.001	1.018	0.112	0.112	0.995	-21.538	43.076	0.067
Std. Err.	0.107	0.102	0.062	0.07	0.07	0.06	8.968	17.937	0.053
Est.	4.969	5.005	1.441	1.04	1.04	1.445	-7.719	15.438	0.028
Std. Err.	0.114	0.114	0.094	0.09	0.09	0.093	8.088	11.175	0.069

Table 2: Point estimate (Est.) and standard error (Std. Err.) values of the parameters of the Gaussian data generating model, with $T = 1000$ observations for all of the three states of the HMM.

	$\boldsymbol{\mu}_k$		$\boldsymbol{\Sigma}_k$				λ	χ	ψ
$K = 1$									
Est.	4.995	4.998	1.506	-1.125	-1.125	1.51	-0.973	1.936	0.002
Std. Err.	0.042	0.042	0.066	0.057	0.057	0.058	0.107	0.256	0.013
$K = 2$									
Est.	-5.003	-4.996	1.5	-1.119	-1.119	1.502	-0.952	1.893	0.002
Std. Err.	0.065	0.067	0.09	0.081	0.081	0.083	0.149	0.379	0.02
Est.	4.99	5.006	1.529	1.159	1.159	1.532	-0.952	1.857	0.002
Std. Err.	0.061	0.063	0.094	0.087	0.087	0.085	0.149	0.378	0.022
$K = 3$									
Est.	-5.011	-4.993	1.491	-1.107	-1.107	1.493	-0.944	1.821	0.002
Std. Err.	0.077	0.081	0.111	0.108	0.108	0.096	0.299	0.56	0.082
Est.	0.002	0.004	1.006	0.123	0.123	1.009	-0.912	1.758	0.003
Std. Err.	0.067	0.068	0.078	0.077	0.077	0.081	0.222	0.504	0.045
Est.	4.982	5.02	1.484	1.103	1.103	1.493	-0.941	1.873	0.003
Std. Err.	0.076	0.081	0.105	0.109	0.109	0.12	0.298	0.569	0.081

Table 3: Point estimate (Est.) and standard error (Std. Err.) values of the parameters of the t data generating model, with $T = 1000$ observations for all of the three states of the HMM.

	$\boldsymbol{\mu}_k$		$\boldsymbol{\Sigma}_k$				λ	χ	ψ
$K = 1$									
Est.	5.002	4.992	1.508	-1.127	-1.127	1.507	-0.501	1.978	0.001
Std. Err.	0.064	0.064	0.062	0.066	0.066	0.061	0.047	0.288	0.001
$K = 2$									
Est.	-4.983	-4.983	1.513	-1.125	-1.125	1.497	-0.484	1.933	0.001
Std. Err.	0.102	0.096	0.084	0.083	0.083	0.089	0.076	0.424	0.001
Est.	4.991	5.011	1.496	1.121	1.121	1.509	-0.483	1.881	0.001
Std. Err.	0.094	0.099	0.09	0.096	0.096	0.101	0.084	0.439	0.002
$K = 3$									
Est.	-4.988	-4.974	1.481	-1.104	-1.104	1.499	-0.481	1.901	0.001
Std. Err.	2.648	3.838	0.16	0.161	0.161	0.143	1.233	3.551	0.022
Est.	-0.012	0	1.018	0.14	0.14	1.001	-0.461	1.8	0.001
Std. Err.	0.327	0.521	0.136	0.231	0.231	0.164	1.638	3.642	0.015
Est.	4.986	5.01	1.497	1.131	1.131	1.523	-0.472	1.834	0.001
Std. Err.	0.119	1.911	0.131	0.144	0.144	0.154	0.212	1.479	0.009

Table 4: Point estimate (Est.) and standard error (Std. Err.) values of the parameters of the Cauchy data generating model, with $T = 1000$ observations for all of the three states of the HMM.

	μ_k		Σ_k			λ	χ	ψ	
$K = 1$									
Est.	4.993	5.008	1.509	-1.13	-1.13	1.505	0.896	0	0.446
Std. Err.	0.049	0.049	0.057	0.053	0.053	0.052	0.12	0.105	0.062
$K = 2$									
Est.	-4.986	-5.002	1.504	-1.116	-1.116	1.493	0.824	0	0.41
Std. Err.	0.072	0.074	0.08	0.085	0.085	0.089	0.165	0.118	0.085
Est.	4.986	5.001	1.496	1.119	1.119	1.505	0.81	0.004	0.401
Std. Err.	0.075	0.074	0.085	0.082	0.082	0.08	0.227	0.26	0.092
$K = 3$									
Est.	-4.988	-4.999	1.511	-1.135	-1.135	1.514	0.754	0.001	0.36
Std. Err.	0.089	0.092	0.108	0.109	0.109	0.099	0.245	0.276	0.119
Est.	-0.007	-0.003	1.007	0.137	0.137	1.012	0.756	0	0.368
Std. Err.	0.07	0.076	0.068	0.076	0.076	0.07	0.188	0.21	0.095
Est.	4.984	5.012	1.476	1.099	1.099	1.496	0.741	0	0.352
Std. Err.	0.092	0.091	0.11	0.105	0.105	0.099	0.271	0.35	0.127

Table 5: Point estimate (Est.) and standard error (Std. Err.) values of the parameters of the Laplace data generating model, with $T = 1000$ observations for all of the three states of the HMM.

is obtained by taking the maximum, $\max_k \gamma_t(k)$, a posteriori probability for every $t = 1, \dots, T$. In Table 8 we report the mean and standard deviation of ARI for the posterior probabilities for the two ($K = 2$) and three-state ($K = 3$) HMGHGMs across the six settings considered. Firstly, we observe that the data generating model plays a fundamental role in estimating the true states partition, as we obtain slightly worst clustering performance for the model with the Cauchy distribution. Secondly, the goodness of the clustering obtained depends, as expected, on the number of states of the Markov chain considered, being the values slightly higher with $K = 2$ than with $K = 3$. Overall, the proposed HMGHGM is able to recover the true state partition highly satisfactory in all the cases examined.

	$\boldsymbol{\mu}_k$		$\boldsymbol{\Sigma}_k$				λ	χ	ψ
$K = 1$									
Est.	4.991	5.005	1.51	-1.12	-1.12	1.501	1.48	2.068	2.849
Std. Err.	0.044	0.042	0.05	0.054	0.054	0.055	2.782	3.666	1.767
$K = 2$									
Est.	-5.003	-4.996	1.042	-0.3	-0.3	1.046	1.889	1.743	2.987
Std. Err.	0.05	0.054	0.052	0.059	0.059	0.057	3.46	4.566	2.461
Est.	4.991	4.999	1.051	0.318	0.318	1.048	1.631	1.563	2.868
Std. Err.	0.054	0.054	0.05	0.049	0.049	0.049	3.136	4.315	1.979
$K = 3$									
Est.	-5	-5	1.486	-1.102	-1.102	1.491	1.883	0.968	2.644
Std. Err.	0.079	0.071	0.088	0.094	0.094	0.101	3.472	4.164	2.69
Est.	-0.01	0.014	1	0.112	0.112	1.012	2.078	1.018	2.854
Std. Err.	0.068	0.065	0.059	0.068	0.068	0.059	3.49	4.286	2.734
Est.	4.995	5.015	1.524	1.144	1.144	1.514	1.793	2.045	2.603
Std. Err.	0.089	0.088	0.106	0.099	0.099	0.103	3.914	4.688	3.203

Table 6: Point estimate (Est.) and standard error (Std. Err.) values of the parameters of the generalized hyperbolic data generating model, with $T = 1000$ observations for all of the three states of the HMM.

	μ_k		Σ_k			λ	χ	ψ	
$K = 1$									
Est.	4.993	4.992	1.509	-1.127	-1.127	1.507	1.393	0.034	0.471
Std. Err.	0.068	0.068	0.053	0.056	0.056	0.053	0.409	1.105	0.093
$K = 2$									
Est.	-5.004	-4.997	1.505	-1.137	-1.137	1.524	1.395	0.013	0.467
Std. Err.	0.101	0.101	0.081	0.081	0.081	0.082	0.625	1.851	0.138
Est.	4.994	5.012	1.515	1.136	1.136	1.511	1.269	0.077	0.428
Std. Err.	0.109	0.105	0.07	0.073	0.073	0.072	0.654	2.142	0.134
$K = 3$									
Est.	-5.02	-4.996	1.501	-1.114	-1.114	1.492	1.297	0.024	0.444
Std. Err.	0.139	0.145	0.09	0.101	0.101	0.107	0.846	2.935	0.184
Est.	-0.005	0.009	1.019	0.128	0.128	0.998	1.231	0.107	0.419
Std. Err.	0.119	0.115	0.074	0.083	0.083	0.073	0.751	2.32	0.204
Est.	4.996	5.011	1.528	1.146	1.146	1.514	1.294	0.022	0.429
Std. Err.	0.132	0.138	0.11	0.095	0.095	0.1	0.893	3.113	0.188

Table 7: Point estimate (Est.) and standard error (Std. Err.) values of the parameters of the variance gamma data generating model, with $T = 1000$ observations for all of the three states of the HMM.

	$K = 2$					
	N	t	C	L	gh	vg
Mean	0.9989	0.9851	0.943	0.9909	0.9999	0.9833
Std. Err.	0.0022	0.0076	0.0157	0.0064	0.0005	0.0081
	$K = 3$					
Mean	0.9322	0.9228	0.7709	0.9059	0.9786	0.8506
Std. Err.	0.0171	0.0165	0.0746	0.0186	0.0087	0.0249

Table 8: Mean and standard error (Std. Err.) values of ARI for the posterior probabilities for Gaussian (N), t, Cauchy (C), Laplace (L), generalized hyperbolic (gh) and variance gamma (vg) with $T = 1000$ for $K = 2$ and $K = 3$.

Scenario 3: Finally, in order to evaluate the ability of the HMGHGM to correctly retrieve the graph structure in each latent state, following [Finegold & Drton \(2011\)](#), we draw a state-specific random 10×10 sparse matrix $\Theta_k = \Sigma_k^{-1}$ according to the following procedure:

- Choose each lower-triangular element of Θ_k independently to be $-1, 0, 1$ with probability 15%, 70% and 15%, respectively;
- For $j > h$ set $\Theta_{k,h,j} = \Theta_{k,j,h}$;
- To ensure positive definiteness of Θ_k , set $\Theta_{k,i,i} = 1 + h$, with h being the number of nonzero elements in the i th row of Θ_k .

As in [Finegold & Drton \(2011\)](#), to strengthen the partial correlations in Θ_k we reduce its diagonal elements by fixing a minimum eigenvalue of 0.6. We then sample $T = 1000$ observations from the data generating models described above (see Table 1) for a one ($K = 1$) and two ($K = 2$) state HMM. For each of the six distributions, we run the proposed HMGHGM on an equispaced grid of 50 values for the tuning parameter ρ from 0.01 to 0.9 with the weight $\nu_k = 1/K$, $k = 1, \dots, K$, assigning the same penalty for all states. For each model, we carry out 50 Monte Carlo replications and assess how well different distributions of the GH family recover the true edges in each state by reporting ROC curves averaged over the 50 replicates and latent states. From left to right, Figure 2 shows the ROC curves, where we plot the true positives rate against the false positives rate for each value of ρ , under the multivariate Gaussian, t, Cauchy, Laplace, generalized hyperbolic and variance gamma multivariate distributions. Overall, these results suggest that when we deal with non-Gaussian heavy tailed data, our static and dynamic graphical models have the same performance of the graphical lasso, representing a robust alternative to existing static approaches and a novelty for dynamic graphical models in non-Gaussian settings.

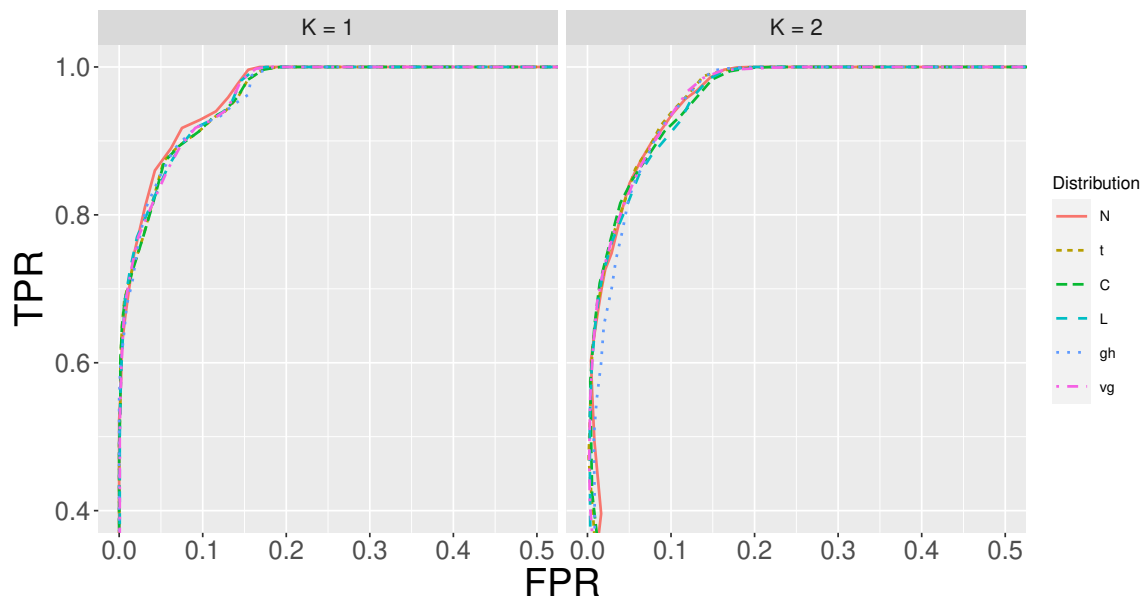


Figure 2: ROC curves for the HMGHGM model under the multivariate Gaussian (N), t , Cauchy (C), Laplace (L), generalized hyperbolic (gh) and variance gamma (vg) distributions for $K = 1$ (left) and $K = 2$ (right) states. Each curve is averaged over 50 Monte Carlo replications. For the two-state model TPR and FPR are obtained as averaged values over the two states.

5 Empirical Application

5.1 Data Description

Over the last decades, hedge fund managers and regulators highlighted the need to accurately assess contagion and systemic risk, depending on the situation of the economy. In this paper, we are interested in investigating how the degree of network connectivity across different asset classes changes in severe market turbulence, which can possibly threaten the integrity of the financial system and represent a potential source of financial instability. For this purpose, we apply the proposed methodology to daily returns of $d = 29$ financial assets comprising stock market indices, commodity futures and digital currencies. The set of considered assets includes the 10 largest cryptocurrencies in terms of market capitalization, including Bitcoin, Ethereum, Ripple and Stellar, the 10 most exchanged metal and energy commodities, such as Gold, Silver, Crude Oil and Natural Gas, and the 9 major world stock indexes, among whom we include the S&P 500, Ftse Mib, Nikkei 225 and the Shanghai Composite Index.

The sample dataset is collected from Yahoo Finance and the study period starts on November 10, 2017 and ends on September 28, 2023, for a total of $T = 1250$ observations after removing missing data. The considered timespan is marked by numerous crises that may have impacted cross-market correlation patterns, spanning from the cryptocurrency bubble crisis in 2017-2018 to the global crisis sparked by the COVID-19 pandemic in 2020-2021, which have caused unprecedented

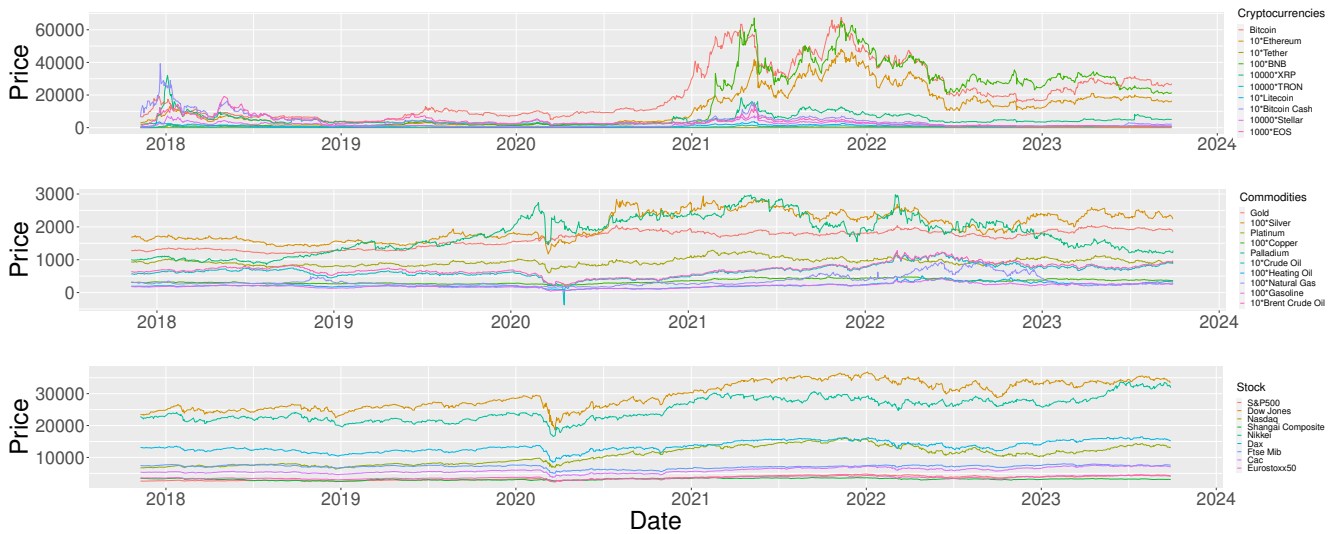


Figure 3: From top to bottom daily time-series of prices of the assets considered. Observations span from November 10, 2017 to September 28, 2023.

levels of uncertainty and risk. Daily returns with continuous compounding are calculated taking the logarithm of the difference between closing prices in consecutive trading days. In Table 9 we report the list of examined variables and the summary statistics for the whole sample. As one can see, each asset displays the typical stylized facts that characterize the financial markets, and cryptocurrencies are generally much more volatile than commodity futures and stock market indices, having the highest standard deviations. Further, the Jarque-Bera test strongly rejects the normality assumption of daily returns for all series considered. Such findings reflect the large price variations, occurred during the period under consideration, which were triggered by the burst of the cryptocurrency bubble in 2018 and by the COVID-19 outbreak at the dawn of 2020. In concluding, the Augmented Dickey-Fuller (ADF) test (Dickey & Fuller 1979) shows that all daily returns are stationary at the 1% level of significance. Figure 3 shows the daily prices of the 29 assets over the entire period of observation. At first glance we immediately recognize the high volatility that characterizes the market of the cryptocurrencies and the waves of exponential price increases. The first wave started at the end of 2018, the first big “bubble” that brought BTC above 20 thousands dollars, another one in mid-2019, and the most recent and bigger one started in late 2020, with a development over the entire course of 2021. As regards commodities and stock indexes, we observe quite a different path with respect to the digital currencies. The collapse of the financial markets at the beginning of 2020 caused by the COVID-19 pandemic represents a watershed for volatility regimes. After March 2020 we see an increase in price volatility for a large proportion of commodities and stock indexes. We also observe price peaks of Gasoline, Crude Oil and Brent during the course of 2022 caused by the sanctions imposed against Russia in response to the Ukrainian war.

Sector	Variable	Minimum	Mean	Maximum	Stdev	Skewness	Kurtosis	Jarque-Bera test	ADF test
Cryptocurrency	1: Bitcoin	-46.47	0.11	22.51	5.03	-0.76	9.01	4343.7	-10.02
	2: Ethereum	-55.07	0.13	32.5	6.47	-0.66	7.73	3203.26	-10.09
	3: Tether	-5.26	0	5.66	0.48	0.77	49.86	129594.27	-14.98
	4: BNB	-54.31	0.38	84.62	7.46	1.19	22.42	26474.64	-9.19
	5: XRP USD	-69.26	0.07	74.65	8.21	1.13	20.88	22976.08	-9.9
	6: TRON	-69.21	0.29	174.43	9.7	5.14	94.96	475117.14	-8.37
	7: Litecoin	-44.91	0	53.98	6.88	0.18	8.55	3811.58	-10.22
	8: Bitcoin Cash	-56.13	-0.08	50.38	8.01	0.21	9.13	4354.43	-10.66
	9: Stellar	-42.96	0.08	80.74	8.06	1.9	20.88	23461.62	-9.94
	10: EOS	-50.42	-0.06	65.12	8.18	0.33	8.78	4041.24	-10.37
Commodities	11: Gold	-5.11	0.03	5.81	1.01	-0.22	4.68	1150.36	-10.5
	12: Silver	-16.08	0.03	14.71	2.02	-0.38	9.08	4324.41	-10.25
	13: Platinum	-12.35	0	11.18	1.99	-0.27	4.07	876.45	-11.32
	14: Copper	-8.14	0.02	6.91	1.55	-0.3	2.26	283.32	-10.93
	15: Palladium	-23.4	0.03	22.6	2.73	-0.43	10.5	5782.71	-12.38
	16: Crude Oil	-28.22	0.09	42.31	3.57	0.99	33.4	58294.49	-8.87
	17: Heating Oil	-26.14	0.06	15.42	2.91	-1.21	13.78	10200.87	-11.36
	18: Natural Gas	-30.05	-0.01	38.17	4.34	0.17	7.92	3270.09	-9.74
	19: RBOB Gasoline	-50.89	0.05	28.88	3.46	-2.51	48.5	123801.84	-9.23
	20: Brent Crude Oil	-27.58	0.06	27.42	2.88	0.09	18.14	17149.08	-9.81
Stock Indexes	21: S&P500	-12.77	0.04	8.97	1.38	-0.94	13.81	10115.35	-10.1
	22: Dow Jones	-13.84	0.03	10.76	1.38	-1.12	18.85	18773.32	-10.4
	23: Nasdaq	-13.15	0.06	8.93	1.62	-0.62	7.07	2682.89	-10.1
	24: Shanghai Composite Index	-8.04	-0.01	7.55	1.17	-0.39	4.98	1324.96	-11.33
	25: Nikkei	-6.27	0.03	7.73	1.27	-0.01	3.48	630.63	-11.02
	26: Dax	-13.05	0.01	10.41	1.37	-0.56	12.89	8715.23	-10.25
	27: Ftse Mib	-11.51	0	8.67	1.15	-1.05	14.21	10741.41	-10.59
	28: Cac	-13.1	0.02	8.06	1.35	-0.92	12.45	8254.22	-10.56
	29: Eurostoxx50	-13.24	0.01	8.83	1.35	-0.88	12.75	8630.23	-10.45

Table 9: Summary statistics of daily log-returns over the entire period. The Jarque-Bera and ADF test statistic is displayed in boldface when the null hypothesis is rejected at the 1% significance level.

5.2 Results

Following these considerations, the proposed HMGHGM can provide insights into the temporal evolution of the conditional correlations of asset returns, where the assets' multivariate distribution is not constrained to be Normal but can assume any fat-tailed distribution within the GH family. As a first step of the empirical analysis, in order to select the optimal ρ in (28) and number of latent states K , we fit the proposed HMGHGM for a sequence of 300 values of ρ for $K = \{1, \dots, 4\}$. We also include a state-specific penalty term by setting the weight ν_k in (28) as the (scaled) effective sample size of state k , i.e., $\nu_k = \sum_{t=1}^T \gamma_t(k)/T$, where $\gamma_t(k)$ is defined in (12). To select the best pair (K, ρ) , we consider two model selection criteria, namely a Bayesian Information Criterion (BIC) type index and the Mixture Minimum Description Length (MMDL, [Figueiredo et al. 1999](#)) defined, respectively, as

$$\text{BIC}_{K,\rho} = -\ell(\boldsymbol{\theta}|\mathbf{y}_1, \dots, \mathbf{y}_T) + \frac{1}{2} \log(T)K(K-1) + \frac{1}{2} \log(T) \sum_{k=1}^K Df(k, \rho) \quad (30)$$

$$\text{MMDL}_{K,\rho} = -\ell(\boldsymbol{\theta}|\mathbf{y}_1, \dots, \mathbf{y}_T) + \frac{1}{2} \log(T)K(K-1) + \sum_{k=1}^K \frac{1}{2} \log(T\nu_k)Df(k, \rho), \quad (31)$$

where $\ell(\boldsymbol{\theta}|\mathbf{y}_1, \dots, \mathbf{y}_T)$ denotes the observed log-likelihood and we set the degrees of freedom as $Df(k, \rho) = d + \sum_{l \geq l'} \mathbf{1}_{\boldsymbol{\theta}_{k,\rho}^{ll'} \neq 0}$. The two criteria are identical, with the only difference that the MMDL adjusts the penalty term for the effective sample size $T\nu_k$ of each state k . The optimal K and ρ are obtained by selecting the model with the lowest criterion value. To compare models with differing number of states, Table 10 reports the BIC and MMDL values for each K at the optimal ρ . As can be seen, the BIC selects 2 states, while MMDL chooses $K = 3$ at the optimal ρ . Following the works of [Figueiredo et al. \(1999\)](#) and [Städler & Mukherjee \(2013\)](#), demonstrating that, in general, the MMDL outperforms the BIC, we thus select the proposed HMGHGM with $K = 3$ states for our analyses.

	$K = 1$	$K = 2$	$K = 3$	$K = 4$
BIC	148657.1	141338.4	141663.0	143774.4
MMDL	148657.1	140635.4	140090.8	141096.8

Table 10: BIC and MMDL values corresponding to the optimal ρ with varying number of states. Bold font highlights the best values for the considered criteria (lower-is-better).

In light of these comments, we begin commenting on the results by the hidden process. The top of the Figure 4 represents the estimated posterior probabilities of being in latent state j , at time t , where $j = 1, \dots, K$ and $t = 1, \dots, T$, conditional on the observed time-series and with over-imposed trend according to a smoothed local regression. These probabilities allow us to make inference on the latent process and to describe the different market phases of the assets considered. The bottom Figure 4 shows the decoded states obtained through local decoding by considering the maximum of the posterior probabilities and the Viterbi algorithm. The two methods convey almost identical results. The predicted trajectories indicate that the three states are visited the 38%, 39% and 23% of the entire period, respectively. Overall, the following conclusions can be drawn. The distribution of states closely mirrors the dynamics of the considered portfolio during the last five years. In particular, State 3 manages to capture the speculative waves of the cryptocurrency market at the end of 2017, in mid-2019, and at the most recent surge during 2021. As can be observed in Figure 3, these periods are characterized by extreme price movements with exponential behaviors and can represent subsequent dramatic losses for the investors. State 1 and 2 instead succeed in mimic the behavior of commodities and stock markets during the considered time frame. State 1, which identifies the period that goes from the end of 2017 to the collapse of financial markets of March 2020 induced by the COVID-19 pandemic, is related to a phase of low prices. State 2 instead indicates the phases of the markets that, after the second half of 2020, are characterized by rise in prices. Overall, Figure 4 suggests us that the proposed model efficiently manages to identify high and low price and volatility trends that alternate over the years.

In order to summarize the interconnectedness among the considered assets during different market conditions, we build the regime-specific graphs $\widehat{G}_k = (V, \widehat{E}_k)$, $k = 1, \dots, K$, where the variables in Table 9 represent the vertices in V , identified by the corresponding estimated precision matrix $\widehat{\Theta}_k$, $k = 1, \dots, K$. Specifically, an edge between two nodes is created in the k -th graph if the estimated $\widehat{\Theta}_{k,i,l} \neq 0$, i.e., $(i, l) \in \widehat{E}_k$ if and only if $\widehat{\Theta}_{k,i,l} \neq 0$, for $i, l \in V, i \neq l$. Figures 5a, 5b and 5c report the estimated graphs for the selected three-states HMGHGM. To highlight the most important variables in the network, pies in light blue indicate the degree centrality measure of each node, while the edge colors specify the sign of the corresponding interaction (green = positive, red = negative). In each graph, stock market indexes are coloured in yellow, cryptocurrencies in grey while commodities are shown in red, and the vertex labels are reported in Table 9. By looking at Figure 5c, each graph identifies a different regime of network connectivity consistently with the remarks given above. We identify a high asymmetry in network connectivity: being State 3 the representation of the speculative waves of the cryptocurrency market, the third graph shows, as expected, a strong centrality and clustering pattern of the crypto assets. The most central nodes (BNB, TRON, Litecoin, Stellar) indeed represents some of the assets with the most “explosive” trends during the crypto bubble. The strong clustering pattern is present across the three estimated graphs. Specifically, digital currencies are strongly tied to each other and rather isolated from other assets (Dyhrberg 2016, Bouri et al. 2017, Corbet et al. 2018, Giudici & Polinesi 2021). It emerges how they might act as safe-haven assets offering protection to investors against losses to offset market risk, being uncorrelated with stocks during market up and downturns. In all three networks, Bitcoin is one of the least central node among the cryptos. This is in line with the work of Bouri et al. (2019), which explains that the behaviour of crypto-traders is not to anchor to a price level: after an exponential price appreciation in one cryptocurrency (e.g., Bitcoin), they start to look for more attractive cryptocurrencies that have a better risk-reward profile. One example is represented by Stellar (9) and Litecoin (7), which result always very central in each state of the chain.

On the other hand, volatility of commodities and stock indexes is closely related to the uncertainty of the economic outlook. As one can see, in the first two states of the chain the most central nodes are represented by stocks (in particular Dow Jones, Nasdaq, Dax and Eurostoxx50) and commodities (i.e. Platinum, Copper, Crude Oil and Gasoline), who have been particularly affected by the interruptions in global production chains over the course of the pandemic. We detect strong clustering patterns for all the three sectors considered. In particular we highlight the strongest connections within metals, energy, European and US indexes, representing possible co-movements during both upward and downward trends, probably due to the fact that assets of the same sectors or indexes of the same regions have responded similarly to the economic crisis caused by the pandemic. Finally, we highlight the role of the Gold as a safe haven asset, being one of the most disconnected nodes in the graph for every volatility level.

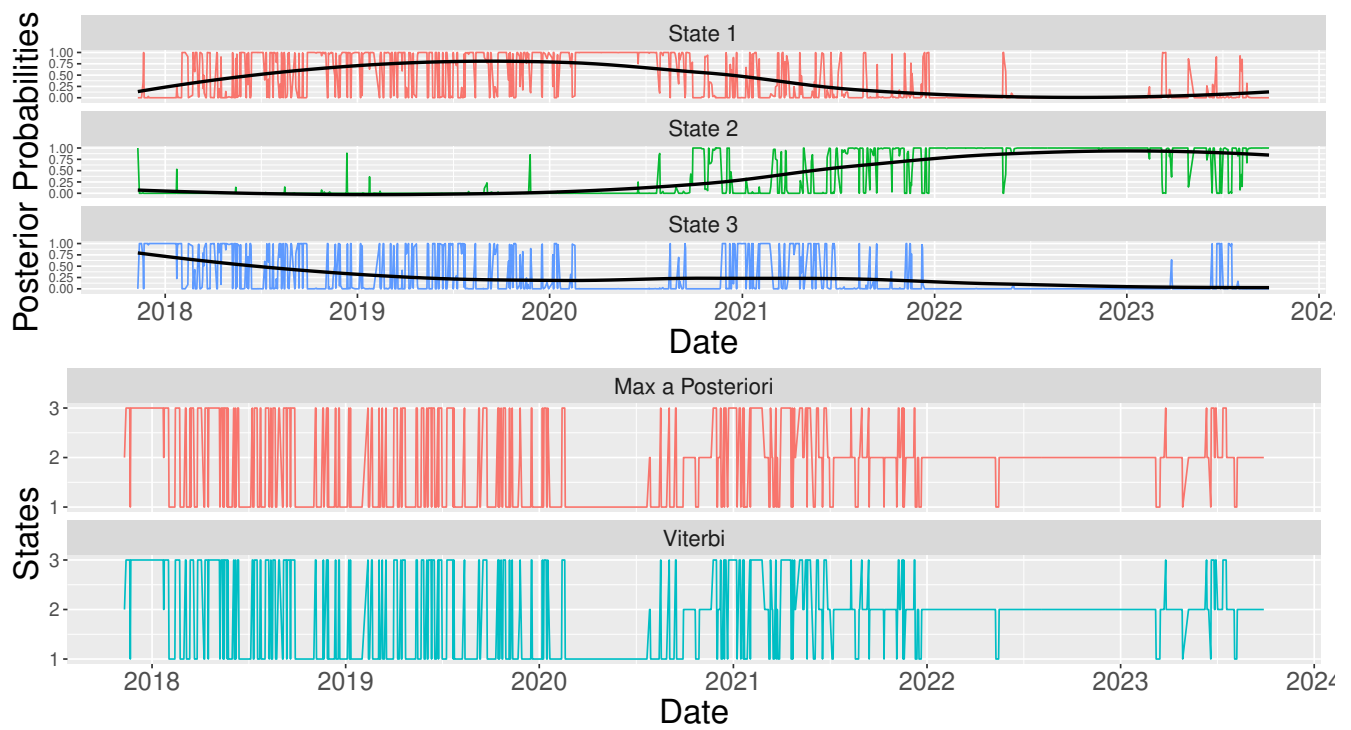


Figure 4: From top to bottom, predicted posterior probabilities and predicted sequence of hidden states over time with $K = 3$ states. The over-imposed black lines denote the trend estimated by a local linear regression.

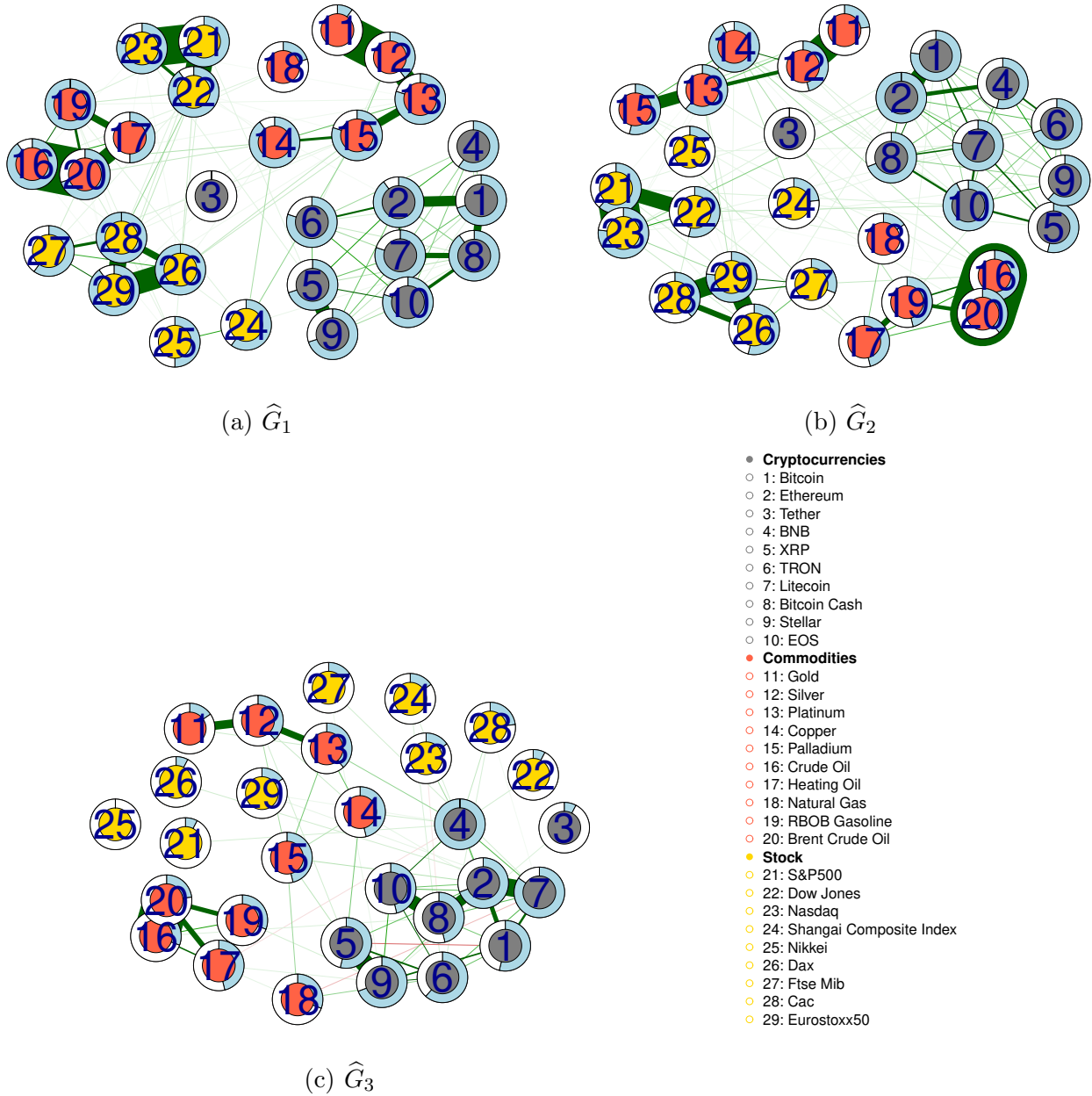


Figure 5: Estimated graphs for $k = 1$ (a), $k = 2$ (b) and $k = 3$ (c). Yellow, grey and red nodes represent respectively indexes, cryptocurrencies and commodities while the vertex labels are illustrated in Table 9. Green edges in the networks depict positive associations, while red edges represent negative associations. Pies in light blue indicate degree centrality.

6 Conclusions

This paper proposes a new sparse dynamic graphical model to study time-varying conditional correlations between important commodities, cryptocurrencies and stock indexes in a period of high volatility and market turbulence, without relying on the assumption of normally distributed data. Starting from [Finegold & Drton \(2011\)](#) and [Städler & Mukherjee \(2013\)](#), we introduce a hidden Markov graphical model where, conditional on the latent state, emission densities follow a (symmetric) GH distribution with state-dependent parameters. Since the index and concentration parameters are completely free to vary within the GH family they allow us to accommodate well a wide range of empirical characteristics of the data in real applications. To induce sparsity and recover only the most prominent relations, we develop a Penalized ECME algorithm exploiting the Gaussian location-scale mixture representation of the GH distribution with a Lasso L_1 penalty on the elements of the state-specific precision matrices. Our procedure is computationally efficient and can be implemented by making use of the *glasso* of [Friedman et al. \(2008\)](#) within the conditional M-step of the proposed algorithm. The good performance of our model is evaluated using numerical simulations under different scenarios.

In the real data analysis we considered daily returns of 29 cryptocurrencies, commodities and market indexes from November 2017 to September 2023 to investigate the dynamics of conditional correlation structure across different financial markets during low and high volatility periods. According to the MMDL criteria, we identified three latent regimes corresponding to different degrees of network connectivity. The first two regimes show negative and positive phases of the market, respectively, while the third manages to capture the peculiar explosive trends of the cryptocurrencies. The estimated graphs are consistent with the hypothesis that cryptocurrencies are highly connected to each other and disconnected from traditional asset types ([Bouri et al. 2017](#), [Corbet et al. 2018](#), [Giudici & Polinesi 2021](#)), resulting in possible safe-haven assets during tumultuous times. Commodities that stand out in terms of degree centrality are the ones that have been the most affected by the interruptions in global production chains over the course of pandemic, namely Palladium, Copper, Crude Oil and Gasoline.

Outside the financial world, for example, a similar methodology could be employed in the field of dynamic mixed graphical models, that could convey critical information when employing not just continuous but also discrete datasets. Future research may also extend the proposed graphical model by using multivariate asymmetric distributions within the GH family.

References

- Bagnato, L., Farcomeni, A. & Punzo, A. (2023), ‘The generalized hyperbolic family and automatic model selection through the multiple-choice lasso’, *arXiv preprint arXiv:2306.08692* .
- Banerjee, O., Ghaoui, L. E. & d’Aspremont, A. (2008), ‘Model selection through sparse maximum

- likelihood estimation for multivariate Gaussian or binary data’, *Journal of Machine Learning Research* **9**(Mar), 485–516.
- Baum, L. E., Petrie, T., Soules, G. & Weiss, N. (1970), ‘A maximization technique occurring in the statistical analysis of probabilistic functions of Markov chains’, *The Annals of Mathematical Statistics* **41**(1), 164–171.
- Baur, D. G., Hong, K. & Lee, A. D. (2018), ‘Bitcoin: Medium of exchange or speculative assets?’, *Journal of International Financial Markets, Institutions and Money* **54**, 177–189.
- Bianchi, D., Billio, M., Casarin, R. & Guidolin, M. (2019), ‘Modeling systemic risk with markov switching graphical SUR models’, *Journal of Econometrics* **210**(1), 58–74.
- Bouri, E., Molnár, P., Azzi, G., Roubaud, D. & Hagfors, L. I. (2017), ‘On the hedge and safe haven properties of Bitcoin: Is it really more than a diversifier?’, *Finance Research Letters* **20**, 192–198.
- Bouri, E., Shahzad, S. J. H. & Roubaud, D. (2019), ‘Co-explosivity in the cryptocurrency market’, *Finance Research Letters* **29**, 178–183.
- Bouri, E., Shahzad, S. J. H. & Roubaud, D. (2020), ‘Cryptocurrencies as hedges and safe-havens for US equity sectors’, *The Quarterly Review of Economics and Finance* **75**, 294–307.
- Bouri, E., Shahzad, S. J. H., Roubaud, D., Kristoufek, L. & Lucey, B. (2020), ‘Bitcoin, gold, and commodities as safe havens for stocks: New insight through wavelet analysis’, *The Quarterly Review of Economics and Finance* **77**, 156–164.
- Browne, R. P. & McNicholas, P. D. (2015), ‘A mixture of generalized hyperbolic distributions’, *Canadian Journal of Statistics* **43**(2), 176–198.
- Brunetti, C., Harris, J. H., Mankad, S. & Michailidis, G. (2019), ‘Interconnectedness in the inter-bank market’, *Journal of Financial Economics* **133**(2), 520–538.
- Cai, T., Liu, W. & Luo, X. (2011), ‘A constrained ℓ_1 minimization approach to sparse precision matrix estimation’, *Journal of the American Statistical Association* **106**(494), 594–607.
- Chatzis, S. P. (2010), ‘Hidden Markov models with nonelliptically contoured state densities’, *IEEE transactions on pattern analysis and machine intelligence* **32**(12), 2297–2304.
- Chen, Y., Giudici, P., Hadji Misheva, B. & Trimborn, S. (2020), ‘Lead behaviour in bitcoin markets’, *Risks* **8**(1), 4.
- Chen, Y., Härdle, W. & Jeong, S.-O. (2008), ‘Nonparametric risk management with generalized hyperbolic distributions’, *Journal of the American Statistical Association* **103**(483), 910–923.

- Corbet, S., Meegan, A., Larkin, C., Lucey, B. & Yarovaya, L. (2018), ‘Exploring the dynamic relationships between cryptocurrencies and other financial assets’, *Economics Letters* **165**, 28–34.
- De Angelis, L. & Paas, L. J. (2013), ‘A dynamic analysis of stock markets using a hidden Markov model’, *Journal of Applied Statistics* **40**(8), 1682–1700.
- Dempster, A. P. (1972), ‘Covariance selection’, *Biometrics* pp. 157–175.
- Dickey, D. A. & Fuller, W. A. (1979), ‘Distribution of the estimators for autoregressive time series with a unit root’, *Journal of the American Statistical Association* **74**(366a), 427–431.
- Drton, M. & Perlman, M. D. (2004), ‘Model selection for Gaussian concentration graphs’, *Biometrika* **91**(3), 591–602.
- Drton, M. & Perlman, M. D. (2008), ‘A sinful approach to Gaussian graphical model selection’, *Journal of Statistical Planning and Inference* **138**(4), 1179–1200.
- Dyhrberg, A. H. (2016), ‘Bitcoin, gold and the dollar—a GARCH volatility analysis’, *Finance Research Letters* **16**, 85–92.
- Fan, J. & Li, R. (2001), ‘Variable selection via nonconcave penalized likelihood and its oracle properties’, *Journal of the American statistical Association* **96**(456), 1348–1360.
- Figueiredo, M. A., Leitao, J. M. & Jain, A. K. (1999), On fitting mixture models, in ‘International Workshop on Energy Minimization Methods in Computer Vision and Pattern Recognition’, Springer, pp. 54–69.
- Finegold, M. & Drton, M. (2011), ‘Robust graphical modeling of gene networks using classical and alternative t-distributions’, *The Annals of Applied Statistics* pp. 1057–1080.
- Froni, B., Merlo, L. & Petrella, L. (2023a), ‘Expectile hidden Markov regression models for analyzing cryptocurrency returns’, *arXiv preprint arXiv:2301.09722* .
- Froni, B., Merlo, L. & Petrella, L. (2023b), ‘Quantile and expectile copula-based hidden Markov regression models for the analysis of the cryptocurrency market’, *arXiv preprint arXiv:2307.06400* .
- Friedman, J., Hastie, T. & Tibshirani, R. (2008), ‘Sparse inverse covariance estimation with the graphical Lasso’, *Biostatistics* **9**(3), 432–441.
- Gao, X. & Massam, H. (2015), ‘Estimation of symmetry-constrained Gaussian graphical models: application to clustered dense networks’, *Journal of Computational and Graphical Statistics* **24**(4), 909–929.

- Giudici, P. & Parisi, L. (2018), ‘Corisk: credit risk contagion with correlation network models’, *Risks* **6**(3), 95.
- Giudici, P. & Polinesi, G. (2021), ‘Crypto price discovery through correlation networks’, *Annals of Operations Research* **299**(1), 443–457.
- Green, P. J. (1990), ‘On use of the EM algorithm for penalized likelihood estimation’, *Journal of the Royal Statistical Society: Series B (Methodological)* **52**(3), 443–452.
- Hubert, L. & Arabie, P. (1985), ‘Comparing partitions’, *Journal of Classification* **2**(1), 193–218.
- Ignatieva, K. & Landsman, Z. (2015), ‘Estimating the tails of loss severity via conditional risk measures for the family of symmetric generalised hyperbolic distributions’, *Insurance: Mathematics and Economics* **65**, 172–186.
- Ji, Q., Bouri, E., Gupta, R. & Roubaud, D. (2018), ‘Network causality structures among Bitcoin and other financial assets: A directed acyclic graph approach’, *The Quarterly Review of Economics and Finance* **70**, 203–213.
- Konlack Socgnia, V., Wilcox, D. et al. (2014), ‘A comparison of generalized hyperbolic distribution models for equity returns’, *Journal of Applied Mathematics* **2014**.
- Lauritzen, S. L. (1996), *Graphical models*, Vol. 17, Clarendon Press.
- Liu, C. & Rubin, D. B. (1994), ‘The ECME algorithm: a simple extension of EM and ECM with faster monotone convergence’, *Biometrika* **81**(4), 633–648.
- Liu, H., Han, F., Yuan, M., Lafferty, J. & Wasserman, L. (2012), ‘High-dimensional semiparametric Gaussian copula graphical models’, *The Annals of Statistics* **40**(4), 2293–2326.
- Liu, H., Lafferty, J. & Wasserman, L. (2009), ‘The nonparanormal: Semiparametric estimation of high dimensional undirected graphs.’, *Journal of Machine Learning Research* **10**(10).
- Liu, H. & Wang, L. (2017), ‘Tiger: A tuning-insensitive approach for optimally estimating gaussian graphical models’, *Electronic Journal of Statistics* **11**(1), 241–294.
- MacDonald, I. L. & Zucchini, W. (1997), *Hidden Markov and other models for discrete-valued time series*, Vol. 110, CRC Press.
- Maruotti, A., Punzo, A. & Bagnato, L. (2019), ‘Hidden Markov and semi-Markov models with multivariate leptokurtic-normal components for robust modeling of daily returns series’, *Journal of Financial Econometrics* **17**(1), 91–117.
- McNeil, A. J., Frey, R. & Embrechts, P. (2015), *Quantitative risk management: concepts, techniques and tools-revised edition*, Princeton university press.

- Meinshausen, N. & Bühlmann, P. (2006), ‘High-dimensional graphs and variable selection with the lasso’, *The Annals of Statistics* **34**(3), 1436–1462.
- Mergner, S. & Bulla, J. (2008), ‘Time-varying beta risk of Pan-European industry portfolios: A comparison of alternative modeling techniques’, *The European Journal of Finance* **14**(8), 771–802.
- Necula, C. et al. (2009), ‘Modeling heavy-tailed stock index returns using the generalized hyperbolic distribution’, *Romanian Journal of Economic Forecasting* **10**(2), 118–131.
- Nystrup, P., Madsen, H. & Lindström, E. (2017), ‘Long memory of financial time series and hidden Markov models with time-varying parameters’, *Journal of Forecasting* **36**(8), 989–1002.
- Pennoni, F., Bartolucci, F., Forte, G. & Ametrano, F. (2022), ‘Exploring the dependencies among main cryptocurrency log-returns: A hidden Markov model’, *Economic Notes* **51**(1), e12193.
- R Core Team (2023), *R: A Language and Environment for Statistical Computing*, R Foundation for Statistical Computing, Vienna, Austria. ISBN 3-900051-07-0.
URL: <http://www.R-project.org/>
- Silva, T. C., da Silva Alexandre, M. & Tabak, B. M. (2018), ‘Bank lending and systemic risk: A financial-real sector network approach with feedback’, *Journal of financial Stability* **38**, 98–118.
- Silva, W., Kimura, H. & Sobreiro, V. A. (2017), ‘An analysis of the literature on systemic financial risk: A survey’, *Journal of Financial Stability* **28**, 91–114.
- Städler, N. & Mukherjee, S. (2013), ‘Penalized estimation in high-dimensional hidden Markov models with state-specific graphical models’, *The Annals of Applied Statistics* pp. 2157–2179.
- Tibshirani, R. (1996), ‘Regression shrinkage and selection via the Lasso’, *Journal of the Royal Statistical Society. Series B (Methodological)* **58**(1), 267–288.
- Welch, L. R. (2003), ‘Hidden Markov Models and the Baum-Welch algorithm’, *IEEE Information Theory Society Newsletter* **53**(4), 10–13.
- Xue, L. & Zou, H. (2012), ‘Regularized rank-based estimation of high-dimensional nonparanormal graphical models’, *The Annals of Statistics* **40**(5), 2541–2571.
- Zhang, C.-H. et al. (2010), ‘Nearly unbiased variable selection under minimax concave penalty’, *The Annals of Statistics* **38**(2), 894–942.
- Zhang, Y., Chu, J., Chan, S. & Chan, B. (2019), ‘The generalised hyperbolic distribution and its subclass in the analysis of a new era of cryptocurrencies: Ethereum and its financial risk’, *Physica A: Statistical Mechanics and its Applications* **526**, 120900.
- Zucchini, W., MacDonald, I. L. & Langrock, R. (2016), *Hidden Markov models for time series: an introduction using R*, Chapman and Hall/CRC.